Highly absorbing black Mg and rare-earth-Mg switchable mirrors

I. A. M. E. Giebels,* J. Isidorsson,† and R. Griessen
Faculty of Sciences, Department of Physics and Astronomy, Condensed Matter Physics, Vrije Universiteit, De Boelelaan 1081, 1081 HV Amsterdam, The Netherlands

(Received 11 December 2003; revised manuscript received 5 March 2004; published 28 May 2004)

Apart from a reflecting and a transparent state, rare-earth-Mg alloys (RE-Mg) exhibit also a highly absorbing, black state during loading with hydrogen. The occurrence of such a black state is due to the disproportionation into subwavelength size $REH_{2+\epsilon}$ and Mg grains during the first hydrogen loading. While the optical properties of REH_x change continuously with a further increase in hydrogen concentration x, Mg changes abruptly from a good reflector to a transparent insulator (MgH_2). Thin pure Mg films also show this black state when (un)loaded carefully at elevated temperatures. By using the Bruggeman effective medium approximation in combination with the transfer matrix method it is shown that the coexistence of Mg and MgH_2 grains is the cause of this high absorption. Furthermore, we compare this phenomenon to the high absorption of light observed in metal-dielectric composites.

DOI: 10.1103/PhysRevB.69.205111 PACS number(s): 78.20.−e, 78.66.−w, 71.30.+h, 73.61.−r

I. INTRODUCTION

Since the discovery of switchable mirrors based on YH_x and LaH_x and rare-earth hydride (REH_x) films[1] a lot of research has been done on this type of materials. The special characteristic of these mirrors is that they can be continuously and reversibly switched between a metallic, reflecting state ($REH_{2+\epsilon}$) and an insulating, transparent state ($REH_{3-\delta}$) by the absorption (or desorption) of hydrogen. This can be done by gasochromic,[1] electrochromic,[2,3] or chemochromic[4] means. Furthermore, they display photochromic,[5] piezochromic,[6] and thermochromic[7] changes in their optical properties. Due to their optical changes, thin films of, e.g., Y can also be used as hydrogen indicators[8,9] in diffusion experiments. Another development is pixel switching, i.e., independent switching of small islands from reflecting to transparent, which can be observed in epitaxial REH_x films.[10,11] This is a very important step for application as display. The most obvious application would be to use them as electrochromic smart windows.[12] The first prototype laboratory devices of switchable mirrors have been made already.[3,13] Since it is possible to dissolve large quantities of hydrogen in metallic and intermetallic compounds, these materials are also interesting for hydrogen storage applications.[14]

In this paper, we focus on pure magnesium and magnesium containing RE metals. Switchable mirrors containing Mg are especially interesting since they can be tailored to be highly reflective in the unloaded state and transparent over the entire optical range[15–18] (i.e., colorless) in their transparent state. Technologically this is a significant improvement upon REH_x that exhibits an optical transmission window in the red ($1.6 \leqslant \hbar\omega \leqslant 2.1$ eV) at hydrogen concentrations $1.7 \leqslant x \leqslant 2.1$ in their reflective state and a transparent state ($REH_{3-\delta}$) with characteristic colors, e.g., yellow for $YH_{3-\delta}$ (absorption edge at 2.6 eV) and red for $LaH_{3-\delta}$ (absorption edge at 1.9 eV).[19]

Apart from a reflecting and a transparent state, these RE-Mg alloys and thin Mg films exhibit also a highly absorbing, black state during loading with hydrogen. This black state has been observed in $Gd_{1-z}Mg_zH_x$ with $z > 0.50$ (Refs. 3,15,20), in $La_{0.5}Mg_{0.5}H_x$ (Ref. 21) and in $Y_{1-z}Mg_zH_x$ alloys. We believe that the black state is a fundamental property of all RE-Mg alloys with a considerable amount of Mg. It has, however, not been studied in detail. The purpose of this paper is to give a quantitative description of the mechanism responsible for the existence of the black state.

Nagengast *et al.*[22] have shown that thin films of RE-Mg alloys disproportionate as soon as they are exposed to hydrogen. During this disproportionation, which is also known for bulk RE-Mg,[23,24] Mg domains act as a microscopic optical shutter when changing from a shiny metal (Mg) to the large band gap insulator[25,26] (MgH_2) upon hydrogenation. The presence of a REH_x (with $1.9 < x < 2.9$) matrix plays only a secondary role. This can be demonstrated by showing that a pure Mg film exhibits also a black state when appropriately loaded with H_2. Thus, the key ingredient is the coexistence of nanograins of Mg and MgH_2.

Furthermore, we show that this phenomenon is similar to the high absorption of light observed in metal-dielectric composites[27,28] such as Au-glass,[29–31] Ag-glass,[32] and Co-Al_2O_3.[33] Its origin is fundamentally different from that of other black materials such as microstructured Si[34] or Ni-P[35] for which a rough surface morphology is essential. The black state observed in Mg_2NiH_x is also of different origin.[36] There a layered growth of the hydride plays an essential role.[37]

II. EXPERIMENT

Polycrystalline LaMg, YMg, and Mg films are evaporated under ultrahigh vacuum conditions (10^{-9} mbar) on quartz substrates and glassy carbon at room temperature and 100 or 300 °C (Mg and RE-Mg, respectively). Y and La are evaporated with an *e*-gun and Mg with a Knudsen effusion cell. To protect the La containing films against oxidation a 1.5 nm thick Al buffer layer is evaporated subsequently.[38] This thin layer is then oxidized to AlO_x in 10^{-5} mbar of O_2 during 1000 s. To promote hydrogen dissociation and absorption a 2.5 to 10 nm thick Pd layer is deposited on top of the films. The evaporation rates and the total thickness are monitored

in situ by a quartz crystal monitor. Afterwards, the film composition is checked *ex situ* with Rutherford backscattering spectrometry (RBS). For RBS measurements samples on glassy carbon substrates are used preferably since the magnesium signal is difficult to assess on a quartz (SiO_2) substrate because of its overlap with the Si signal.

Structural measurements are performed in a Rigaku x-ray diffractometer using Cu K_α radiation in a θ-2θ configuration. The dynamic x-ray experiments are monitored in a relatively limited angular range, usually with 2θ between 26° and 41° with a scan time of approximately 8 min per spectrum.

Optical transmission and reflection spectra at near-normal incidence are recorded in a Bruker IFS 66/S Fourier transform infrared spectrometer in the range $[0.72\ \text{eV} < \hbar\omega < 3.5\ \text{eV}]$ (i.e., 1722–354 nm). Reflection spectra are measured from the backside of the samples through the substrate to circumvent the reflection of the metallic Pd cap layer.

The films are slowly hydrogenated (pressures lower than 1 bar of H_2) at room temperature or 50 to 100 °C for Mg in order to follow the optical changes *in situ* in detail. The resistivity is monitored *in situ* as well. For this, the sample is contacted with four 30 μm thick Al wires by means of an ultrasonic bonding machine and connected to a Keithley 2000 multimeter. We use Van der Pauw's method[39] to determine the resistivity.

III. RESULTS

A. Structure

1. RE-Mg films

From x-ray diffraction (XRD) measurements on YMg-H_x and LaMg-H_x films[21] at room temperature we arrive at the following scenario for the hydrogenation of RE-Mg alloys. RE-Mg alloys (except Yb-Mg) deposited in a 1 to 1 ratio form an intermetallic compound with the CsCl structure. However, when RE-Mg compounds (both in bulk[23,24] and in thin film form[21,22,40,41]) such as LaMg, CeMg, YMg, and GdMg are exposed to hydrogen they disproportionate. This is due to the great hydrogen affinity of RE metals that form dihydrides already at very low pressures (10^{-29} bar for Y films[42] and 10^{-33} bar for Gd films[40] at room temperature). Thus, the CsCl intermetallic compound of RE-Mg, when exposed to hydrogen, immediately disproportionates into $REH_{2+\epsilon}$ and Mg, which are both reflecting. In the fully hydrogenated state $REH_{3-\delta}$ and MgH_2 coexist. Both are transparent. In between these two extreme states both $REH_{2+\epsilon}$ and Mg change from reflecting (metallic) to transparent (insulating). However, they do this in a different way. For example YH_x does not undergo a structural phase transition between the dihydride and trihydride phases if more than 10 at. % Mg is added as was shown already by Van der Molen *et al.*[16] Thus, both YH_x and LaH_x stay fcc between $x=2$ and $x=3$ and their optical properties change gradually with hydrogen concentration.[19] Magnesium however, is hcp in the metallic phase and tetragonal (rutile)[43,44] or orthorhombic[44,45] in the insulating MgH_2 phase. Thus, magnesium forms MgH_2 grains (with a structural phase transition), whose volume fraction increases with increasing H uptake. The switching of $REH_{2+\epsilon}$ to $REH_{3-\delta}$ and Mg to MgH_2 occurs at essentially the same hydrogen pressure as was shown by Di Vece *et al.*[40] for GdMg alloys and by Giebels *et al.*[18] for Y/Mg multilayers. Thus, the enthalpy of formation of REH_3 is very close to that of MgH_2. Furthermore, there are indications that MgH_2 is in the orthorhombic γ-phase when Mg is embedded in a matrix of YH_x (Ref. 22) and rutile (α-phase) in a matrix of LaH_x.[21]

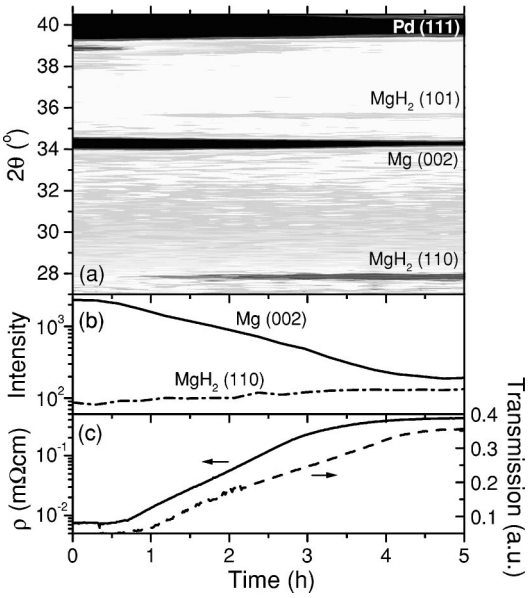

FIG. 1. *In situ* x-ray diffraction during hydrogenation at 100 °C of a 188 nm thick Mg film on quartz covered with 10 nm Pd. (a) Contour plot of the XRD spectra, (b) intensity of the hcp Mg (002) peak and the rutile MgH_2 (110) peak, and (c) resistivity ρ and transmission of the same sample. The time is given in hours. At $t=0.3$ h 10 mbar of hydrogen is applied. It is increased to 36 mbar H_2 at $t=0.72$ h.

2. Mg films

Recently, we have succeeded to load thin films of Mg to MgH_2 at elevated temperatures and pressures.[25] This is not straightforward since palladium capped Mg films exhibit unusual kinetics due to the formation of a blocking MgH_2 layer at the interface between Pd and Mg.[46,47] The MgH_2 layer prevents H to diffuse to the metallic Mg that is still present underneath. The formation of this blocking layer can be circumvented by hydrogenation at a temperature of 50–100 °C. In Fig. 1 the evolution of the x-ray spectra during loading with hydrogen is given together with the resistivity and transmission of a 188 nm thick Mg film covered with 10 nm Pd. The sample is hydrogenated at 100 °C. At 39.95° the (111) peak of fcc Pd is observed. The (002) peak of hcp Mg is seen at 34.4°. Two peaks corresponding to rutile MgH_2 appear at 35.7° (101) and 27.9° (110). However, only 90% of the Mg can be switched to MgH_2 at 100 °C and a pressure of 1 bar H_2. With a pressure of 100 bars the film can be fully loaded to MgH_2.[25] Using the Debye-Scherrer formula we can determine the x-ray coherence length which is an esti-

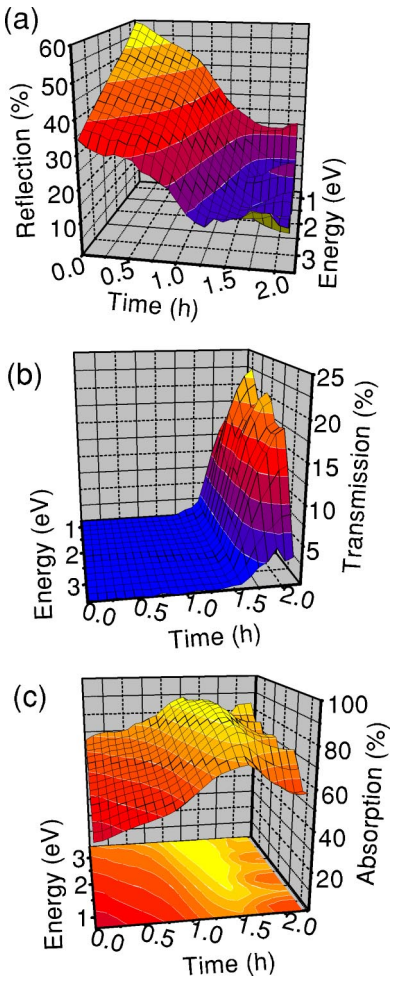

FIG. 2. (Color online) (a) Reflection, (b) transmission, and (c) absorption of a 200 nm YMg film on quartz covered with 10 nm Pd during loading in 10 mbar H_2. The time is given in hours. At $t=2.2$ h the sample is fully loaded with hydrogen. The overall composition is then approximately YMg-$H_{4.9}$.

mate for the grain size. For a Mg sample deposited at room temperature the grain size is 27 nm, after hydrogenation the grain size decreases to about 23 nm.

B. Optical behavior

Figures 2(a) and 2(b) show the reflection and transmission of a 200 nm thick YMg film on quartz covered with 10 nm Pd during loading at 10 mbar H_2. This low hydrogen pressure is chosen for a slow hydrogenation of the sample. From the measured reflection, R, and transmission, T, we calculate the absorption, A, with $A=1-R-T$ [see Fig. 2(c)]. Apart from a reflecting and a transparent state it is clear that there exists a highly absorbing, black state as well. This black state is not only observed during hydrogen absorption but also during desorption and is independent of the rate of hydrogen loading. The black state, which corresponds to the hill in A, occurs when the reflection is low and the film is just becoming transparent. Over the entire visible part of the spectrum the absorption is 85–90%. In Fig. 3 spectra around this highly absorbing state are shown. One should note that the

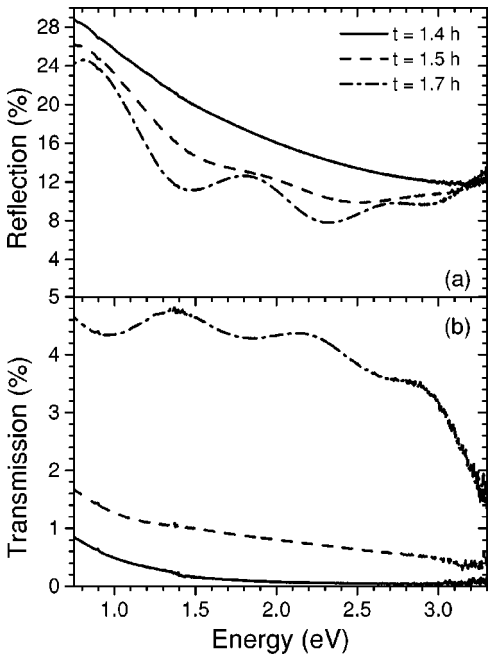

FIG. 3. (a) Reflection and (b) transmission spectra of a 200 nm YMg film on quartz covered with 10 nm Pd around its black state (see Fig. 2 between 1.4 and 1.7 h).

large absorption in the fully hydrogenated sample ($t=2.2$ h in Fig. 2) is due to the metallic Pd cap layer that limits the transmission and is thus not an intrinsic property of YMg-H_x.

After correction for the Pd cap layer and the quartz substrate there is still 70–80 % absorption left in the visible part of the optical spectrum. This is exceptionally high since we are looking (through the transparent substrate) at the smooth interface between the substrate and the film (and not at a rough surface such as in microstructured Si[34] or Ni-P black[35]). Moreover, it is not a narrow absorption line but it spans a wide energy range from the UV to the near-infrared. The same is observed in LaMg films on quartz covered with a 1.5 nm AlO_x/2.5 nm Pd protecting stack.[21] As this high absorption was also reported for GdMg alloys,[3,15] we believe that it is a general feature of RE-Mg alloys with Mg playing a major role. Furthermore, this high optical absorption is also present in Mg/Y and Mg/Ni multilayers.[48]

This triggered us to investigate thin pure Mg films in detail. When hydrogenated carefully at temperatures between 50 and 100 °C thin films of Mg can indeed have a highly absorbing, black state as well. At room temperature and when the films are too thick Mg shows a layered hydrogenation from the top to the bottom. In that case the optical properties are very different. Thus, in order to observe the black state it is very important that the film is loading (or unloading) homogeneously, i.e., MgH_2 (or Mg) nucleates everywhere in the sample. In Fig. 4 the reflection, transmission and absorption of a 100 nm thick Mg film covered with 10 nm Pd is given during unloading at 100 °C in air. Spectra around this highly absorbing state are shown in Fig. 5. We observe the same features as in YMg and LaMg. The total absorption (without correction) is 75–90% from the near-infrared to the ultraviolet.

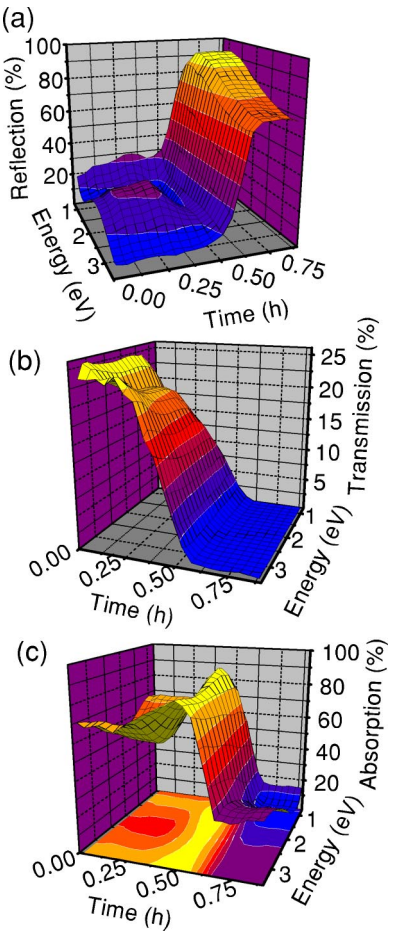

FIG. 4. (Color online) (a) Reflection, (b) transmission, and (c) absorption of a 100 nm Mg film on quartz covered with 10 nm Pd during unloading at 100 °C in air.

C. Resistivity

The resistivity is monitored simultaneously both during XRD and optical measurements. As deposited LaMg and YMg have a resistivity of about 0.1 m Ω cm (including Pd) typical for La and Y. Mg has a resistivity of only 6.5 $\mu\Omega$ cm. The Pd top layer stays metallic during hydrogen loading. Therefore, it is shunting the resistivity of the underlying REMg-H_x or MgH_x layer. The maximum resistivity obtained for the total stack in LaMg (with 1.5 nm AlO_x/2.5 nm Pd) is 1.02 m Ω cm (see Fig. 6) and for Mg (with 10 nm Pd) only 0.39 m Ω cm (see Fig. 7). At the black state the structural data indicate that Mg is transforming to MgH_2 both in RE-Mg films[21] and in Mg (see Fig. 1). The resistivity data are almost featureless in contrast to RE films without Mg.[19] When the resistivity suddenly increases around $t=750$ s (i.e., when the material goes from metallic to insulating), the reflection drops rapidly and the black state develops. This points to percolation phenomena in our films.

IV. MODELING

A. Effective medium theory

Since RE-Mg intermetallic compounds disproportionate upon hydrogen loading into small nanosized grains, our material is a heterogeneous mixture of REH_x, Mg, and MgH_2. To model the optical properties of such a mixture we use the Bruggeman effective medium approximation[49] (BA). This (self-consistent) approximation is able to model absorption over a large wavelength range and gives good results near the percolation threshold.[32,27,31] In this model

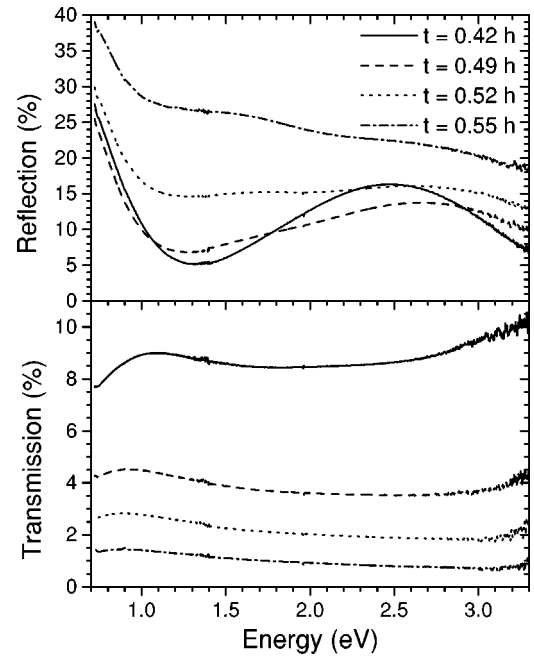

FIG. 5. (a) Reflection and (b) transmission spectra of a 100 nm Mg film on quartz covered with 10 nm Pd around its black state (see Fig. 4 between 0.42 and 0.55 h).

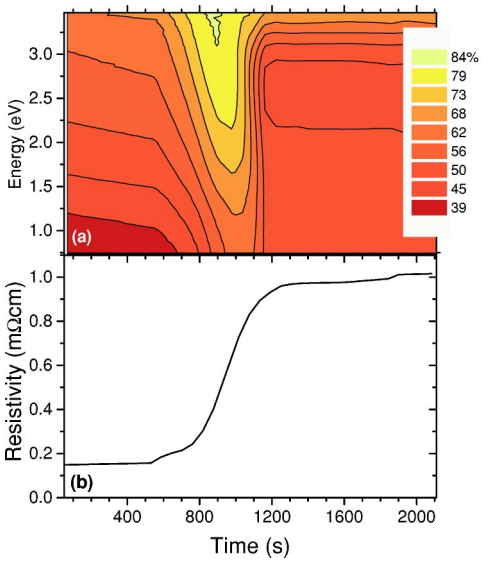

FIG. 6. (Color online) (a) Contour plot of the optical absorption of a 50 nm LaMg film on quartz covered with a 1.5 nm AlO_x/2.5 nm Pd protecting layer. At $t=530$ s 52 mbar hydrogen is applied, at $t=1850$ s the pressure is increased to 1 bar H_2. The scale varies between 40 and 90 % absorption in 9 steps. (b) The resistivity ρ which is measured simultaneously with the optical absorption.

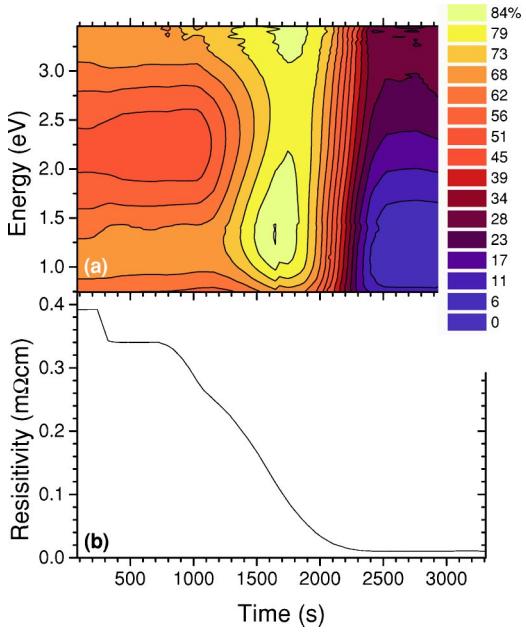

FIG. 7. (Color online) (a) Contour plot of the optical absorption of a 100 nm Mg film on quartz covered with 10 nm Pd during unloading at 100 °C in air. At $t=300$ s the gas cell is evacuated, at $t=790$ s the sample is exposed to ambient air. The scale varies between 0 and 90 % absorption in 16 steps. (b) The resistivity ρ which is measured simultaneously with the optical absorption.

$$f_m\frac{\epsilon_m-\langle\epsilon\rangle}{L\epsilon_m+(1-L)\langle\epsilon\rangle}+f_d\frac{\epsilon_d-\langle\epsilon\rangle}{L\epsilon_d+(1-L)\langle\epsilon\rangle}=0, \qquad (1)$$

where $\langle\epsilon\rangle,\epsilon_m,\epsilon_d$ are the complex dielectric functions $[\epsilon(\omega)=\epsilon_1(\omega)+i\epsilon_2(\omega)]$ of the effective medium, and inclusions of types m (metallic) and d (dielectric), in the host, respectively, and where f_m,f_d represent volume fractions of materials of types m,d in the total volume. L is a geometrical factor which depends on the particle shape. The underlying assumptions are (i) ellipsoidal inclusions, and (ii) dipole polarization only, near-field effects are neglected. Furthermore,

$$f_m+f_d=1.$$

There are several solutions of which only one is physical since $\langle\epsilon_2\rangle$ must always be larger than zero.

In this paper we assume that the inclusions are spheroids with a rotation axis perpendicular to the film plane. This is adequate since our films exhibit out-of-plane texture. The depolarization factors are related to the semiaxis a,b,c via the eccentricity e. For prolate (cigar-shaped) spheroids $c\geqslant a=b$ and for oblate (pancake-shaped) spheroids $c\leqslant a=b$. As in our experiments the optical properties are measured at perpendicular incidence of the light (i.e., electric-field in-plane) the relevant depolarization factor L is for the electric field perpendicular to the rotation axis of the ellipsoid. For prolate spheroids[50]

$$L=\frac{1}{2e^2}-\frac{1-e^2}{4e^3}\ln\left(\frac{1+e}{1-e}\right), \qquad (2)$$

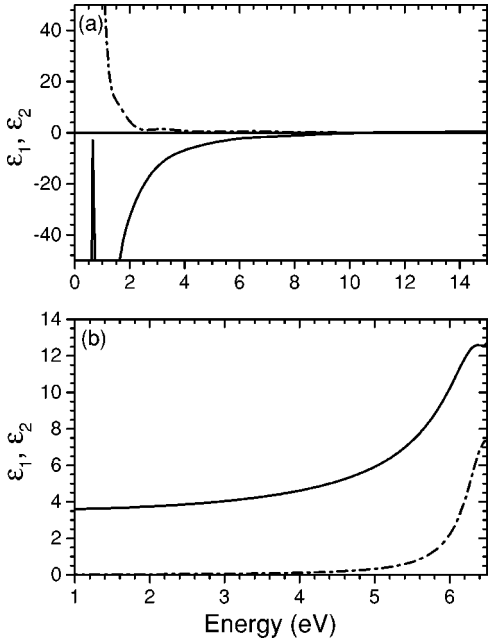

FIG. 8. Real (solid line) and imaginary part (dashed dotted line) of the dielectric function of (a) Mg (Ref. 52) and (b) MgH_2 (Ref. 25) used in the present effective medium calculations.

$$e^2=1-\left(\frac{a}{c}\right)^2, \qquad (3)$$

and for oblate spheroids

$$L=-\frac{1}{2e^2}+\frac{1+e^2}{2e^3}\arctan e, \qquad (4)$$

$$e^2=\left(\frac{a}{c}\right)^2-1, \qquad (5)$$

For spheres $e=0$ and $L=\frac{1}{3}$. $L=0.5$ corresponds to cylinders.

The transfer matrix method[51] is used to calculate the reflection, transmission and absorption of a sample from its effective dielectric function determined with the Bruggeman approximation. The dielectric function used for Mg is taken from Palik's handbook.[52] The effective (bulk) plasmon energy where ϵ_1 crosses zero is $\hbar\omega_p=10.7$ eV for Mg. For MgH_2 we succeeded very recently in determining the dielectric function for the rutile α-phase.[25] α-MgH_2 is an insulator with a band gap of 5.6 ± 0.1 eV. Since calculations show that the optical properties of the orthorhombic γ-phase are almost the same[26] as that of the α-phase we use here the measured dielectric function for MgH_2. The real and imaginary parts of the dielectric function of Mg and MgH_2 used in this work are displayed in Fig. 8.

B. Black state

As it is well known that large absorptions can occur in metal-dielectric composites we assume that a similar situation occurs in RE-Mg hydride. As mentioned above, the introduction of H into RE-Mg leads to a segregation in Mg,

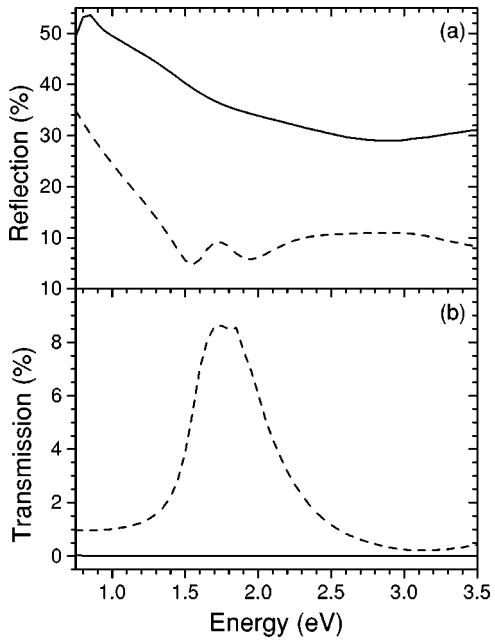

FIG. 9. Reflection (a) and transmission (b) of a 200 nm thick $YMgH_x$ film covered with 10 nm Pd calculated for two different situations when a metal and a semiconductor are combined: Mg-$YH_{2.9}$ (solid line) and MgH_2-$YH_{2.1}$ (dashed line). These results are very different from the experimental data given in Fig. 3.

MgH_2, and REH_x. Mg and REH_2 are metallic, while MgH_2 and $REH_{2.9}$ are semiconducting. The question is then which metal-semiconductor composite is most absorbing and resembles the measurements. First, the combinations of Mg with $LaH_{2.9}$ or $YH_{2.9}$, and the combinations of MgH_2 with $LaH_{2.1}$ or $YH_{2.1}$ are considered (see Fig. 9 for $YMgH_x$). However, none of these combinations gives a black state as observed experimentally (see Fig. 3). If Mg and $REH_{2.9}$ coexist the transmission is zero and the reflection is too high, when MgH_2 and $REH_{2+\epsilon}$ coexist a transmission window around 1.8 eV appears that is not observed in our experiments.

Since there are clear indications that the coexistence of Mg with MgH_2 is crucial for the observed highly absorbing state both in REMg-H_x and in MgH_x (see Secs. III A and III C), the combination of Mg with MgH_2 without the RE material is now considered. The results for a 50 nm thick Mg-MgH_2 composite in vacuum with $L=\frac{1}{3}$ are shown in Fig. 10 where the data are plotted as a function of the volume fraction of MgH_2 and the photon energy. This time a highly absorbing state is indeed observed with an absorption up to about 80% at high photon energies. Since Mg is a very good reflector, the absorption is very low at 100 vol% Mg ($f_d=0$). When 0 vol% Mg is reached (i.e., 100 vol% MgH_2, $f_d=1$) the film is highly transparent[25] and thus the absorption is low again. Note that the calculation is without Pd. As we expect the black state to be related to a percolation phenomenon (see Sec. IV C) we calculated the dielectric function $\langle\epsilon\rangle$ of a Mg-MgH_2 composite for f_m values close to $\frac{1}{3}$ for spherical inclusions (see Fig. 11). When the metallic fraction $f_m<0.35$, the metallic character of the film cannot be seen any longer optically since $\epsilon_1>0$ for all photon energies. If we assume that our film is homogeneous and calculate from the transmission and reflection spectra how the dielectric function looks like in the black state it turns out that it is positive over the entire wavelength range. Thus, we conclude experimentally that f_m must be smaller than 0.35 in the black state (if the inclusions are spherical).

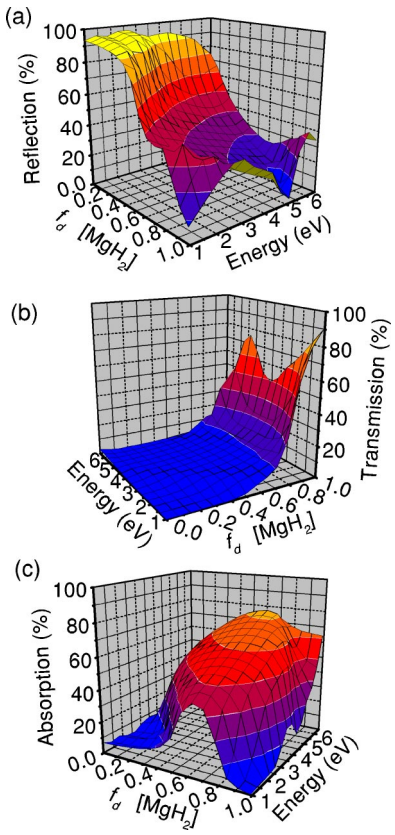

FIG. 10. (Color online) Calculated (a) reflection, (b) transmission, and (c) absorption of a 50 nm thick Mg-MgH_2 composite as a function of the volume fraction of MgH_2 (f_d[MgH_2]) in the Bruggeman approximation between 1 and 6.5 V (no substrate and no Pd cap layer are taken into account). In these calculations the composite is assumed to consist of spherical grains.

When the quartz substrate and the Pd cap layer are taken into account (see Fig. 12) the calculated absorption reproduces nicely the experimental data for $YMgH_x$ [see Fig. 2(c)] as well as $LaMgH_x$ especially in the fully loaded state. Now, there is considerable absorption in the end state ($f_d=1$, 100 vol% MgH_2) due to the Pd cap layer. In the original state ($f_d=0$, 100 vol% Mg) the absorption is still low since we look at the sample from the substrate side. In the experiment, however, the RE material is present as well. This material (Y or La) is not as reflecting as Mg. Therefore, the overall reflection decreases and the absorption increases especially in the unloaded state.

The results obtained for pure Mg films can be reproduced if we assume that 10 at.% of the Mg is not switched to MgH_2 which is in agreement with the XRD data (see Sec. III A). We assume that a thin layer of 10 nm Mg is present below the Pd cap layer of 10 nm. Isidorsson *et al.* have shown that even when no Mg peak is observed in XRD any-

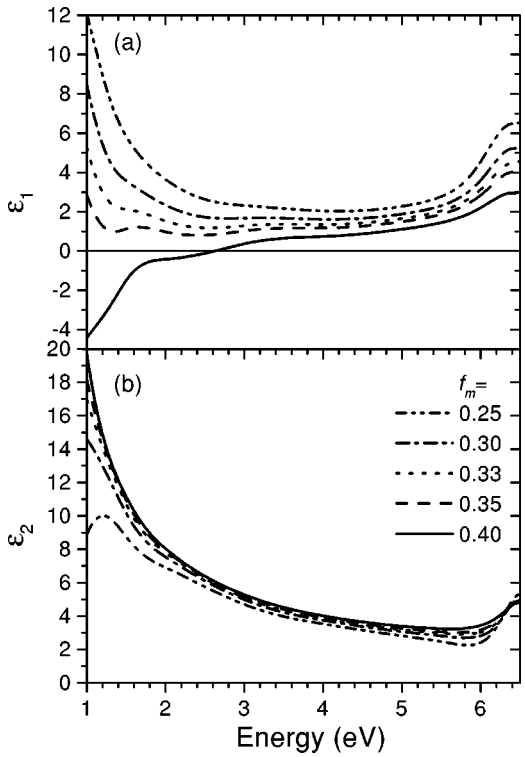

FIG. 11. (a) Real and (b) imaginary parts of the dielectric function of a Mg-MgH_2 composite when the metallic fraction (i.e., volume fraction of Mg) is close to its percolation value $f_m = \frac{1}{3}$. All curves are calculated for spherical grains ($L = \frac{1}{3}$) with the Bruggeman approximation.

more there is still a top layer of about 20 nm thickness that is a mixture between Pd and Mg.[25]

In the Bruggeman approximation we can also explore the effect of the shape of the inclusions on the optical properties. In Fig. 13 the contour plots of the absorption for a Mg-MgH_2 composite is shown for $L = 0.2, \frac{1}{3}$, and 0.5 [see Eqs. (2) and (4)]. These values correspond to c/a ratios for the spheroidal grains of 0.44, 1, and ∞, respectively. For spherical inclusions ($L = \frac{1}{3}$) the maximum absorption at each photon energy occurs at the same volume fraction of MgH_2 (about 0.66). This is indicated by the vertical dashed line in Fig. 13(b). For L values different from $\frac{1}{3}$ the contour plots are skewed. For $L = 0.2$ the volume fraction corresponding to maximum absorption decreases from 0.8 to 0.5 with increasing photon energy. For $L = 0.5$ it increases from 0.5 to 0.8. In Figs. 2(c) and 6(a) it can be seen that in our experiments the maximum absorption also varies with photon energy. As the hydrogen uptake is approximately linear in time this implies that $0.2 < L < \frac{1}{3}$ is compatible with the experimental results. The asymmetry of the absorption contour plots in Figs. 2(c), 6(a), and 7(a) can be used for a rough estimate of L. We find $L \approx 0.24$ for LaMg, $L \approx 0.28$ for YMg and $L \approx 0.31$ for Mg. This corresponds to oblate spheroidal inclusions with $(c/a) \simeq 0.5, 0.7$ and 0.9, respectively. Thus, in pure Mg films the grains are close to spherical.

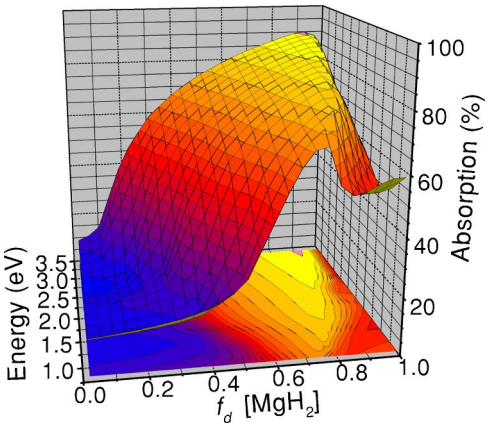

FIG. 12. (Color online) Calculated absorption of a 200 nm thick Mg-MgH_2 composite on quartz and covered with 10 nm Pd in the Bruggeman approximation. As in our experiments (see Fig. 2) the photon energy is chosen between 1 and 3.5 eV.

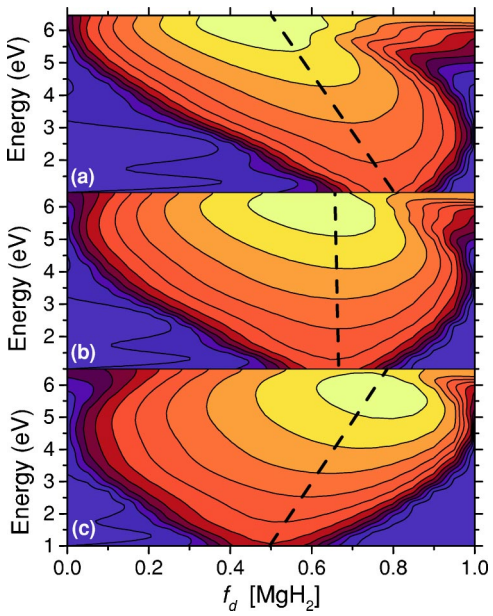

FIG. 13. (Color online) Contour plots of the absorption of a 50 nm thick Mg-MgH_2 composite for $L = 0.2$ (a), $\frac{1}{3}$ (b), and 0.5 (c) which corresponds to oblate ellipsoidal, spherical and cylindrical shaped grains. The scale varies between 0 and 80% absorption in 12 steps. The dashed lines are guides to the eye. They indicate the maximum absorption.

C. Percolation

So far we have focussed on the optical properties of the Mg-MgH_2 composite. As Mg is a metal and MgH_2 an insulator we expect also large changes in the electrical resistivity. A marked change occurs near the percolation limit p_c. For $f_m < p_c$ there is no longer an electrically conducting path of metallic grains in the material. The same relation as for the dielectric function [Eq. (1)] holds as well for the electrical conductivity σ since this is the real part of the dielectric function at zero frequency. Intuitively one expects that the percolation threshold depends on the particle shape. This is indeed true for the Bruggeman approximation.[53] The electrical percolation threshold p_c occurs when

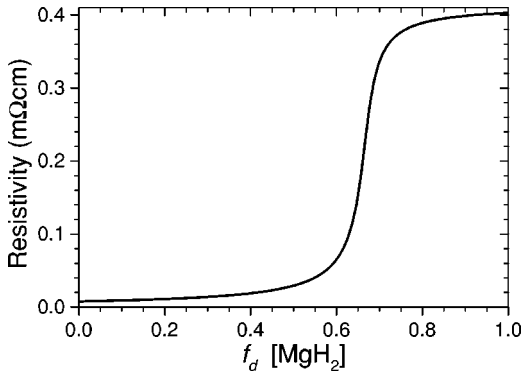

FIG. 14. Electrical resistivity of a 90 nm thick Mg-MgH_2 composite capped with 20 nm Pd-Mg for spherical grains ($L=\frac{1}{3}$) as a function of the volume fraction of MgH_2 (f_d[MgH_2]). The resistivity of the Mg-MgH_2 layer is calculated with the Bruggeman approximation. A double layer model with 20 nm Pd-Mg with a resistivity of 75 $\mu\Omega$ cm in parallel with 90 nm Mg-MgH_2 is used to simulate the experiments (see Fig. 7).

$\omega \rightarrow 0: f_m = p_c = L$.[54,27] This electrical threshold is also observed in the optical absorption at low energies when $\omega \rightarrow 0$ (see Fig. 13). In practice the BA overestimates the value of the percolation threshold and gives too low values for σ for $f_m < p_c$.

To simulate the experiments on pure Mg [see Fig. 7(b)] we have calculated the resistivity (i.e., $1/\sigma$) for a 90 nm thick Mg-MgH_2 composite capped with 20 nm Pd-Mg. In Fig. 14 the result is shown as a function of the volume fraction MgH_2 for spherical grains ($L=\frac{1}{3}$). Mg has a resistivity of 6.5 $\mu\Omega$ cm[25] and the resistivity of MgH_2 is assumed to be 10 mΩ cm. For the Pd-Mg cap layer we take $\rho = 75\mu\Omega$ cm. The agreement between the calculation and the experiment is quite good.

In our measurements of the resistivity of YMg and LaMg films during loading with hydrogen we can also clearly see a transition from a metal to a nonmetal [see Fig. 6(b)]. The large optical absorption is observed in this transition regime. However, the CsCl REMg compound has a much larger resistivity than Mg: 0.1 mΩ cm instead of 6.5 $\mu\Omega$ cm. After disproportionation $YH_{2+\epsilon}$ and $LaH_{2+\epsilon}$ will also take up hydrogen and the resisitivity will increase as well.

V. DISCUSSION

Our calculations show that the key ingredient for the observed high absorption is the coexistence of small Mg and MgH_2 grains. Since this black state is also observed in multilayers with Mg (Ref. 48) and in pure Mg films, the RE material is not playing a major role. The RE material serves to disproportionate the film into small grains of $REH_{2+\epsilon}$ and Mg during the first hydrogen loading. These small grains can switch independently and do not suffer from the kinetic limitations as in pure Mg films.[46] Thus, in RE-Mg films the transition from Mg to MgH_2 takes place throughout the whole film at the same time. In thin Mg-MgH_2 films this is also possible but only at elevated temperatures.

An effective medium approximation is only applicable when the grain size is much smaller than the wavelength of light. In RE-Mg alloys this is indeed the case. Van der Molen *et al.*[16] determined the x-ray coherence length l_{coh} of YH_3 grains in $Y_{1-z}Mg_z$ alloys. It decreases with increasing Mg content from $l_{coh}=18$ nm when $z=0$ to $l_{coh}=4$ nm when $z=0.3$. Unfortunately MgH_2 is hardly visible with x-ray diffraction when Y or La is present. Probably the MgH_2 grains are comparable in size to the YH_3 grains. In (annealed) $La_{0.5}Mg_{0.5}$ alloys the coherence length is about 17 nm for LaH_3 and 13 nm for MgH_2.[21] Di Vece *et al.*[41] conclude that in $Gd_{0.4}Mg_{0.6}$ loaded with hydrogen Gd hydride forms nanometer sized clusters. Thus, for both YMg, LaMg, and GdMg alloys the grain size is much smaller than the wavelength of light. As we have seen in Sec. III A the grain size in pure Mg films is 27 nm for Mg and 23 nm for MgH_2 which is also much smaller than the wavelength of light.

In the literature many examples of metal-dielectric composites can be found. For several cermets both the optical properties and resisitivity have been studied extensively as a function of the volume percentage metal in an insulator. For systems such as Pt-Al_2O_3 (Ref. 27), Au on glass,[29,30] and Co-Al_2O_3 (Ref. 33) large absorption has been reported in the transition regime around the percolation threshold. The shape and magnitude of the effective dielectric functions found for Pt-Al_2O_3 (Ref. 27) and Co-Al_2O_3 (Ref. 33) cermets are quite similar to what we find for YMg hydride or Mg-MgH_2. However, the dielectric properties for Au-MgO (Ref. 27) and Ag-SiO_2 composites are somewhat different since resonances can clearly be seen in the visible part of the optical spectrum.[55,32] This gives rise to a dip in ϵ_1 and a bump in ϵ_2.

The unique feature of our system is that it can switch from a metallic, reflecting system via the black, highly absorbing state at the percolation threshold to a transparent and insulating material by simply changing the hydrogen concentration in our samples. In all other cermets a new sample is needed for each volume percentage of metal in the dielectric.

A. The origin of the large absorption

It is interesting to study in composites the role of the dielectric material and of the metal in their optically highly absorbing state. To investigate the effect of the dielectric material, the optical absorption of a Mg-ideal glass composite is calculated using the Bruggeman approximation and the transfer matrix method (see Sec. IV A) and compared to Mg-MgH_2. For Mg the dielectric function given by Palik[52] is again used, for ideal glass we take $\epsilon_1=2.2$ and $\epsilon_2=0$ over the whole energy range (0.1–20 eV). In the case of MgH_2 we use the calculated dielectric function by Alford and Chou[26] since it covers a wider energy range than the one we measured. The only difference with the measured dielectric function is a shift of 0.5 eV to higher energies so that the calculated gap is 6.1 eV instead of 5.6 eV.[25] In Fig. 15 the contour plots of the absorption as a function of the volume fraction dielectric material f_d is plotted both for (a) Mg-MgH_2 and (b) Mg-ideal glass. The major difference is observed at energies larger than 6.1 eV where MgH_2 has its direct band gap in *GW* calculations.[26] Above this energy photons can be absorbed in MgH_2, thereby exciting electrons from the valence to the conduction band. As a consequence the optical con-

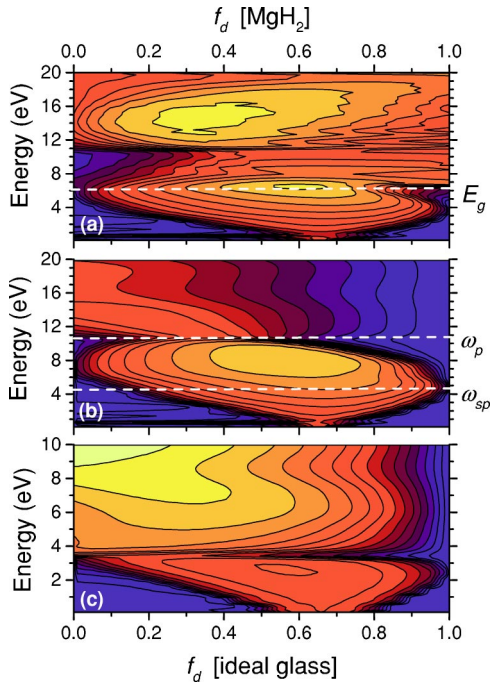

FIG. 15. (Color online) Contour plots of the absorption in a 50 nm thick film in vacuum for various composites: (a) Mg-MgH$_2$ (Ref. 26), (b) Mg-ideal glass, and (c) Ag-ideal glass as calculated with the Bruggeman approximation for $L=\frac{1}{3}$. The scale varies between 0 and 90 % absorption in 16 steps. Indicated are the band gap of MgH$_2$ (E_g), the (effective) bulk plasmon resonance of Mg (ω_p) and the surface plasmon resonance of Mg grains (ω_{sp}).

trast between the metal and dielectric material vanishes at these energies. Therefore, the absorption is decreasing again above this energy in Mg-MgH$_2$ whereas the absorption is still increasing in Mg-ideal glass (see Fig. 15). In Mg-ideal glass the contrast and thus the absorption vanishes above the (effective) plasmon energy of Mg ($\hbar\omega_p=10.7$ eV) where ϵ_1 crosses zero.

The Bruggeman approximation shows on the basis of the dielectric function of a metal and a dielectric what the absorption of a composite would be. It does not give information about the origin of the absorption. It is however well known that surface plasmons exist at a certain frequency on small metallic particles (with a diameter much smaller than the wavelength of light). For spheroids, it follows from both electrostatics and Mie theory that the dipole resonance or surface plasmon ω_{sp} (which is strongest) is present at the photon energy where

$$\epsilon_{1,m}=\epsilon_{1,d}\left(1-\frac{1}{L}\right), \tag{6}$$

if ϵ_2 is small compared to ϵ_1, where m stands for the metal and d for the dielectric medium.[56] This resonance can clearly be observed in calculations of Mg-ideal glass at low volume fractions of Mg at 4.8 eV [see Fig. 15(b)]. The absorption is maximum at energies (just) above the surface plasmon energy and drops rapidly when approaching the (effective) bulk plasma energy ω_p.

For comparison the absorption of a Ag-ideal glass composite which is studied extensively in literature is shown in Fig. 15(c). The dielectric function for Ag is taken from the handbook of Palik.[52] The maximum absorption reached in this system is about 55% whereas in Mg-ideal glass an absorption up to 85% is observed. Using Eq. (6) we can estimate the photon energy of the surface plasmon resonance to be 3.0 eV. The bulk plasmon resonance is 3.8 eV. However, $\epsilon_2=0.75$ and this is not so small compared to ϵ_1. This is due to the fact that Ag is not a free-electron metal like Mg. Silver has a relatively flat d-band from which a lot of interband transitions are possible. Therefore, the corresponding features are observed at lower energies than estimated.

At the percolation threshold, the light induced oscillating dipoles (surface plasmons) of different particles interact with each other forming collective optical excitations in the whole system. Because of the self-similarity of percolating clusters, every size of resonating clusters is present in a sample, and then every interaction length is active, giving rise to a wide plasmon spectrum near the percolation threshold.[28] This is the cause of the absorption at p_c from the IR to the (bulk) plasmon energy (often in the UV) in metal-dielectric composites near percolation (see Fig. 15 at $f_d=0.66$).

Strong disorder in these metal-dielectric composites gives rise to strong localization of the surface plasmons in nanometer-sized regions around the percolation threshold. These resonances induce strong fluctuations of the local electric and magnetic fields that significantly exceed the applied fields. The fluctuations can lead as well to a corresponding enhancement of various nonlinear effects. For example surface plasmons in silver aggregates give rise to strong surface enhanced Raman scattering.[57] Shalaev and Sarychev[58] developed a theory to calculate the local electromagnetic fields in metal-dielectric films and are able to reconstruct the large absorption in these composites around the percolation threshold. However, they can model absorptions up to 50% only. Furthermore, they investigated various nonlinear optical properties of these kind of films. So called ''hot spots,'' spikes in electric (and magnetic) fields are indeed observed recently in gold-on-glass films using scanning optical near-field microscopy.[59,28] These films also show strongly enhanced second-harmonic generation.[60] It can be expected that these phenomena also exist in our Mg films and RE-Mg alloys.

VI. CONCLUSIONS

A rare-earth-Mg alloy with a considerable amount of Mg exhibits the three fundamental optical states of matter, i.e., reflecting, absorbing, and transparent as a function of hydrogen loading. In thin Mg films this can also be observed when the sample is carefully hydrogenated at elevated temperatures. Important is that MgH$_2$ starts to nucleate everywhere in the sample instead of the usually observed layered hydrogenation. The optical properties are continuously and reversibly tunable by simply changing the surrounding hydrogen gas pressure. This is a great advantage above conventional metal-dielectric films. The highly absorbing, black state in RE-Mg films is shown to be closely related to the coexist-

ence of Mg and MgH_2 nanograins. The high absorption occurs when the changes in the resistivity are large. By using Bruggeman's effective medium approximation in combination with the transfer-matrix method it is shown that a combination of Mg and MgH_2 grains gives indeed rise to a high optical absorption. The role of the RE material is to disproportionate the film into small grains of $REH_{2+\epsilon}$ and Mg during the first hydrogen loading. These small grains can switch independently and do not suffer from kinetic limitations as in Mg films. The bulk plasmon frequency of the metal determines at what photon energy the absorption due to cluster resonances vanishes. It is expected that our Mg films and RE-Mg alloys exhibit various nonlinear optical effects just as other metal-dielectric compounds.

ACKNOWLEDGMENTS

The authors are grateful to N. J. Koeman, R. J. Westerwaal, and J. H. Rector for technical support. W. Lohstroh is acknowledged for stimulating discussions. This work is part of the research program of the Stichting voor Fundamenteel Onderzoek der Materie (FOM), financially supported by the Nederlandse Organisatie voor Wetenschappelijk Onderzoek (NWO).

*Corresponding author. Electronic address: giebels@nat.vu.nl

†Present address: Solid State Physics, Uppsala University, Box 534, SE-751 21 Uppsala, Sweden.

[1] J.N. Huiberts, R. Griessen, J.H. Rector, R.J. Wijngaarden, J.P. Dekker, D.G. de Groot, and N.J. Koeman, Nature (London) **380**, 231 (1996).

[2] P.H.L. Notten, M. Kremers, and R. Griessen, J. Electrochem. Soc. **143**, 3348 (1996).

[3] R. Armitage, M. Rubin, T. Richardson, N. O'Brien, and Y. Chen, Appl. Phys. Lett. **75**, 1863 (1999).

[4] P. van der Sluis, Electrochim. Acta **44**, 3063 (1999).

[5] A.F.Th. Hoekstra, A.S. Roy, T.F. Rosenbaum, R. Griessen, R.J. Wijngaarden, and N.J. Koeman, Phys. Rev. Lett. **86**, 5349 (2001).

[6] R.J. Wijngaarden, J.N. Huiberts, D. Nagengast, J.H. Rector, R. Griessen, M. Hanfland, and F. Zontone, J. Alloys Compd. **308**, 44 (2000).

[7] I.A.M.E. Giebels, S.J. van der Molen, R. Griessen, and M. Di Vece, Appl. Phys. Lett. **80**, 1343 (2002).

[8] F.J.A. den Broeder, S.J. van der Molen, M. Kremers, J.N. Huiberts, D.G. Nagengast, A.T.M. van Gogh, W.H. Huisman, N.J. Koeman, B. Dam, J.H. Rector, S. Plota, M. Haaksma, R.M.N. Hanzen, R.M. Jungblut, P.A. Duine, and R. Griessen, Nature (London) **394**, 656 (1998).

[9] A. Remhof, S.J. van der Molen, A. Antosik, A. Dobrowolska, N.J. Koeman, and R. Griessen, Phys. Rev. B **66**, 020101(R) (2002).

[10] J.W.J. Kerssemakers, S.J. van der Molen, N.J. Koeman, R. Günther, and R. Griessen, Nature (London) **406**, 489 (2000).

[11] B.J. Kooi, E. Zoestbergen, J.Th.M. De Hosson, J.W.J. Kerssemakers, B. Dam, and R.C.C. Ward, J. Appl. Phys. **91**, 1901 (2002).

[12] D.R. Rosseinsky and R.J. Mortimer, Adv. Mater. **13**, 783 (2001).

[13] V.M.M. Mercier and P. van der Sluis, Solid State Ionics **145**, 17 (2001).

[14] L. Schlapbach and A. Züttel, Nature (London) **414**, 353 (2001).

[15] P. van der Sluis, M. Ouwerkerk, and P.A. Duine, Appl. Phys. Lett. **70**, 3356 (1997).

[16] S.J. van der Molen, D.G. Nagengast, A.T.M. van Gogh, J. Kalkman, E.S. Kooij, J.H. Rector, and R. Griessen, Phys. Rev. B **63**, 235116 (2001).

[17] P. van der Sluis, Appl. Phys. Lett. **73**, 1826 (1998).

[18] I.A.M.E. Giebels, J. Isidorsson, E.S. Kooij, A. Remhof, N.J. Koeman, J.H. Rector, A.T.M. van Gogh, and R. Griessen, J. Alloys Compd. **330-332**, 875 (2002).

[19] A.T.M. van Gogh, D.G. Nagengast, E.S. Kooij, N.J. Koeman, J.H. Rector, R. Griessen, C.F.J. Flipse, and R.J.J.G.A.M. Smeets, Phys. Rev. B **63**, 195105 (2001).

[20] R. Griessen, Phys. Bl. **53**, 1207 (1997).

[21] J. Isidorsson, I.A.M.E. Giebels, E.S. Kooij, N.J. Koeman, J.H. Rector, A.T.M. van Gogh, and R. Griessen, Electrochim. Acta **46**, 2179 (2001).

[22] D.G. Nagengast, A.T.M. van Gogh, E.S. Kooij, B. Dam, and R. Griessen, Appl. Phys. Lett. **75**, 2050 (1999).

[23] B. Darriet, M. Pezat, A. Hbika, and P. Hagenmuller, Int. J. Hydrogen Energy **5**, 173 (1980).

[24] D. Sun, F. Gingl, Y. Nakamura, H. Enoki, M. Bououdina, and E. Akiba, J. Alloys Compd. **333**, 103 (2002).

[25] J. Isidorsson, I.A.M.E. Giebels, H. Arwin, and R. Griessen, Phys. Rev. B **68**, 115112 (2003).

[26] J. A. Alford and M. Y. Chou (unpublished).

[27] S. Berthier, Ann. Phys. (Paris) **13**, 503 (1988).

[28] P. Gadenne and J.C. Rivoal, Top. Appl. Phys. **82**, 185 (2002).

[29] P. Gadenne, Thin Solid Films **57**, 77 (1979).

[30] P. Gadenne, Y. Yagil, and G. Deutscher, J. Appl. Phys. **66**, 3019 (1989).

[31] F. Brouers, J.P. Clerc, G. Giraud, J.M. Laugier, and Z.A. Randriamantany, Phys. Rev. B **47**, 666 (1993).

[32] C.G. Granqvist and O. Hunderi, Phys. Rev. B **18**, 2897 (1978).

[33] G.A. Niklasson and C.G. Granqvist, J. Appl. Phys. **55**, 3382 (1984).

[34] C. Wu, C.H. Crouch, L. Zhao, J.E. Carey, R. Younkin, J.A. Levinson, E. Mazur, R.M. Farell, P. Gothoskar, and A. Karger, Appl. Phys. Lett. **78**, 1850 (2001).

[35] R.J.C. Brown, P.J. Brewer, and M.J.T. Milton, J. Mater. Chem. **12**, 2749 (2002).

[36] J. Isidorsson, I.A.M.E. Giebels, R. Griessen, and M. Di Vece, Appl. Phys. Lett. **80**, 2305 (2002).

[37] W. Lohstroh, R. J. Westerwaal, B. Noheda, S. Enache, I. A. M. E. Giebels, B. Dam, and R. Griessen (unpublished).

[38] A.T.M. van Gogh, S.J. van der Molen, J.W.J. Kerssemakers, N.J. Koeman, and R. Griessen, Appl. Phys. Lett. **77**, 815 (2000).

[39] L.J. van der Pauw, Philips Res. Rep. **13**, 1 (1958).

[40] M. Di Vece, S.J.M. Zevenhuizen, and J.J. Kelly, Appl. Phys. Lett. **81**, 1213 (2002).

[41] M. Di Vece, A.M.J. van der Eerden, J.A. van Bokhoven, S. Lemaux, J.J. Kelly, and D.C. Koningsberger, Phys. Rev. B **67**, 035430 (2003).

[42] E.S. Kooij, A.T.M. van Gogh, and R. Griessen, J. Electrochem. Soc. **146**, 2990 (1999).

[43] F.H. Ellinger, C.E. Holley, Jr., B.B. McInteer, D. Pavone, R.M.

Potter, E. Staritzky, and W.H. Zachariasen, J. Am. Chem. Soc. **77**, 2647 (1955).
[44] J.P. Bastide, B. Bonnetot, J.M. Létoffé, and P. Claudy, Mater. Res. Bull. **15**, 1215 (1980).
[45] M. Bortz, B. Bertheville, G. Böttger, and K. Yvon, J. Alloys Compd. **287**, L4 (1999).
[46] A. Krozer and B. Kasemo, J. Less-Common Met. **160**, 323 (1990).
[47] J. Rydén, B. Hjörvarsson, T. Ericsson, E. Karlsson, A. Krozer, and B. Kasemo, J. Less-Common Met. **152**, 295 (1989).
[48] I. A. M. E. Giebels, W. Lohstroh, M. Bjurman, and R. Griessen (unpublished).
[49] D.A.G. Bruggeman, Ann. Phys. (Leipzig) **24**, 636 (1935).
[50] L. D. Landau, E. M. Lifschitz, and L. P. Pitaevskiĭ, *Electrodynamics of Continous Media*, 2nd ed., Landau and Lifschitz course of theoretical physics Vol. 8 (Pergamon Press, Oxford, 1993).
[51] M. Born and E. Wolf, *Principles of Optics* (Cambridge University Press, Cambridge, 1980).
[52] *Handbook of Optical Constants of Solids*, edited by E. D. Palik (Academic Press, San Diego, 1998), Vol. I-III.
[53] R. Landauer, AIP Conf. Proc. **40**, 2 (1978).
[54] F. Brouers, J.P. Clerc, and G. Giraud, Phys. Rev. B **44**, 5299 (1991).
[55] E.B. Priestley, B. Abeles, and R.W. Cohen, Phys. Rev. B **12**, 2121 (1975).
[56] C. F. Bohren and D. R. Huffman, *Absorption and Scattering of Light by Small Particles* (Wiley, New York, 1983).
[57] M. Moskovits, L.-L. Tay, J. Yang, and T. Haslett, Top. Appl. Phys. **82**, 215 (2002).
[58] V.A. Shubin, A.K. Sarychev, J.P. Clerc, and V.M. Shalaev, Phys. Rev. B **62**, 11 230 (2000).
[59] S. Grésillon, L. Aigouy, A.C. Boccara, J.C. Rivoal, X. Quelin, C. Desmarest, P. Gadenne, V.A. Shubin, A.K. Sarychev, and V.M. Shalaev, Phys. Rev. Lett. **82**, 4520 (1999).
[60] M. Breit, V.A. Podolskiy, S. Grésillon, G. von Plessen, J. Feldmann, J.C. Rivoal, P. Gadenne, A.K. Sarychev, and V.M. Shalaev, Phys. Rev. B **64**, 125106 (2001).